Supporting Information

Why does Sulfite Reductase employ Siroheme?

Adrian M.V. Brânzanic[1, 2], **Ulf Ryde**[3], **Radu Silaghi-Dumitrescu**[1]

[1] *Department of Chemistry, Babeș-Bolyai University, Cluj-Napoca , Romania.*

[2]*Institute of Interdisciplinary Research in Bio-Nano-Sciences, Babeș-Bolyai University, Cluj-Napoca, Romania.*

[3]*Department of Theoretical Chemistry, Lund University, Lund, Sweden.*

SiR active site models

The siroheme–cubane assembly was extracted from the sulfite reductase crystal structure (PDB entry 1AOP). The peripheral substituents found on the siroheme moiety were replaced by hydrogen atoms for simplicity. The cysteine residues connecting the cubane with the siroheme cofactor and the rest of the protein were modeled as methylthiolate groups (Figure 2 in main text). The two single bonds that differentiates siroheme from heme were desaturated and giving the heme–cubane system (Figure 2 in main text). The (siro)heme Fe ion was modelled in the high-spin ferric state. In terms of magnetic coupling, the two cofactors were arranged with both ferro- and antiferromagnetic alignment.

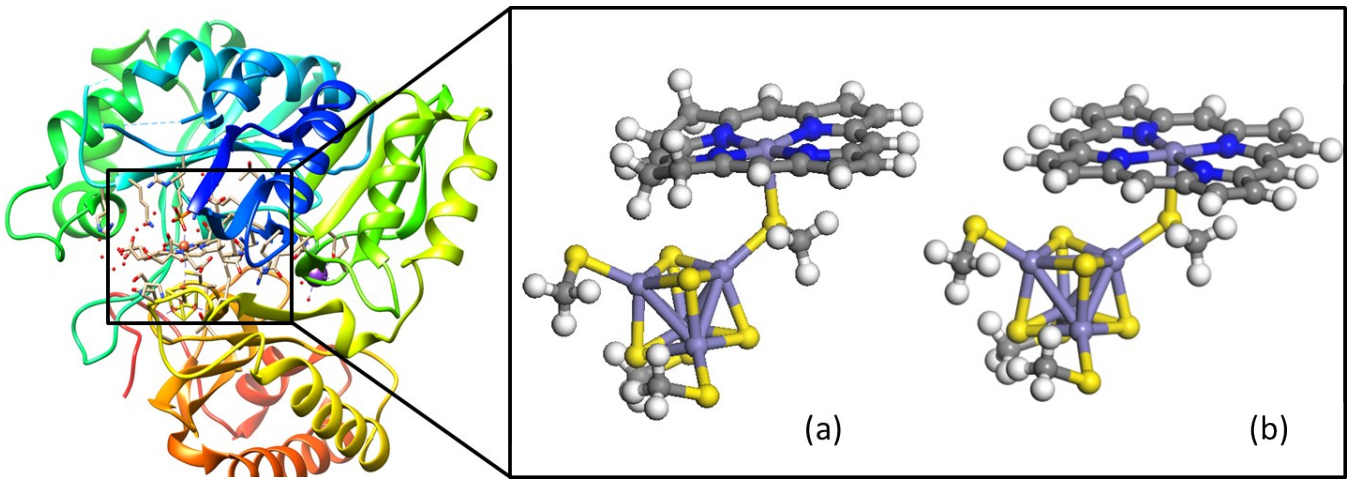

Figure S1. Left: ribbon diagram of sulfite reductase (PDB code: 1AOP). Right: close view of the modeled active site, composed of a siroheme connected to an iron–sulfur [4Fe-4S] cluster via a cysteinate sulfur (a). In model (b) the siroheme cofactor is replaced by heme. Fe is represented in violet, N in blue, S in yellow, O in red, C in grey and H in white.

Electron-transport device models

The obtained (siro)heme–cubane models, together with the corresponding isolated heme, siroheme and cubane components, were used to build electron transport devices. In such assemblies, the molecule of interest is treated as a junction that connects two metal nanorods. The molecular junction is referred to as the island part of the device, while the metal nanorods represent the electrodes. All electron-transport devices that were build consist of gold electrodes (Figure S2) in which the island part of the device is modeled either as heme (Figure S2a), siroheme (Figure S2b), heme–cubane (Figure S2c), siroheme–cubane Figure S2d). Sulfur is commonly used as the atom that connects the island to the electrode part of the device. Likewise, sulfur atoms were added in the axial positions of heme and siroheme models, faced towards the electrodes. For the (siro)heme–cubane systems, the distal axial position (bound to the (siro)heme iron) was similarly occupied by a sulfur atom, while the methyl groups were removed from all methylthiolate residues except for the one connecting the two cofactors. Thus, all island parts from each transport device were connected to the electrodes via sulfur atoms. The distances between the island part and the electrodes were set at 2.5 Å, which represents the experimentally known distance at which sulfur is known to adhere to gold electrodes.[1]

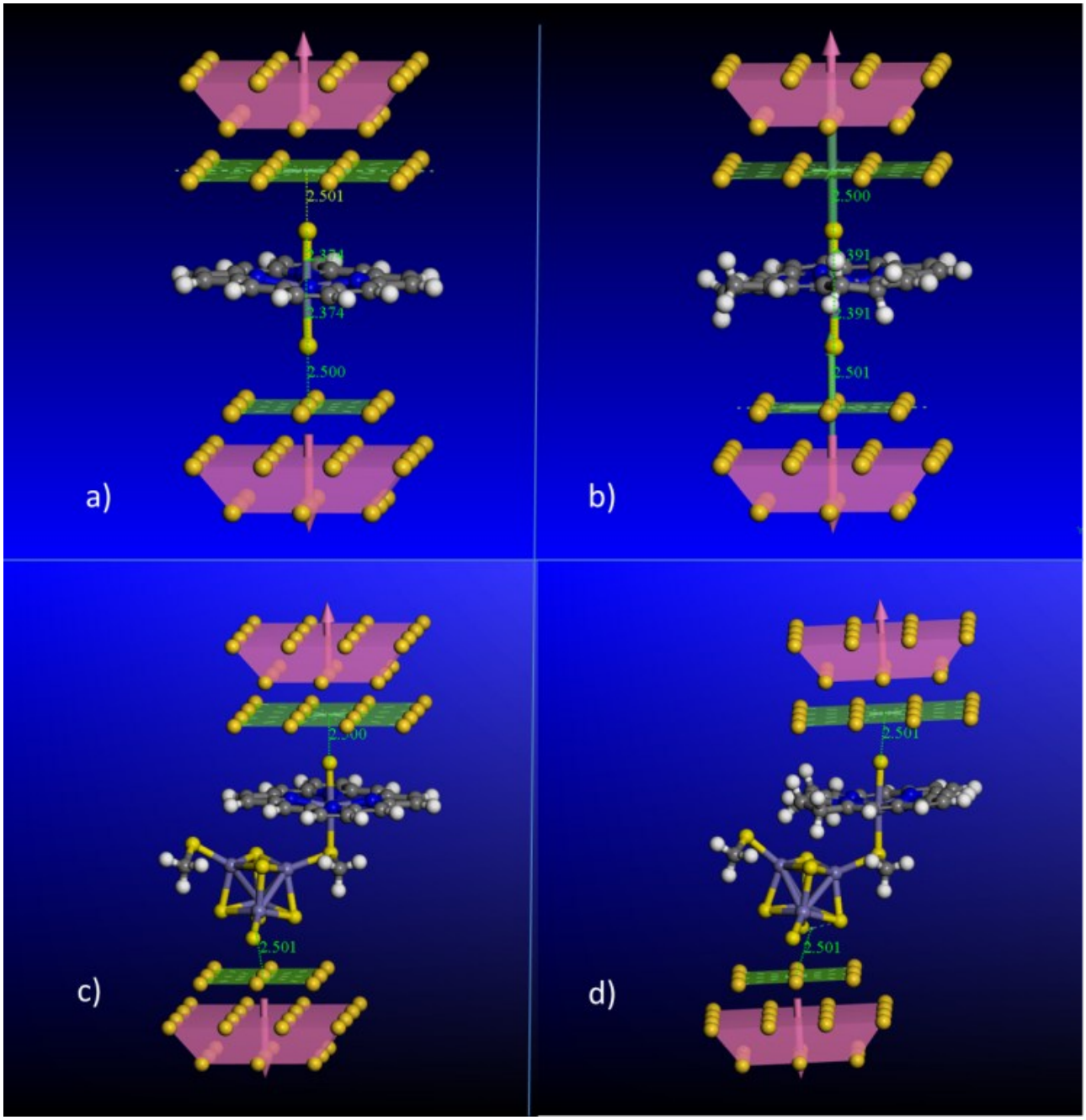

Figure S2. Heme (a), siroheme (b), heme–cubane (c) and siroheme–cubane (d) as molecular junctions connecting two Au electrodes. Au atoms are depicted in dark yellow, Fe in violet, N in blue, S in yellow, O in red, C in grey and H in white.

Methods

1. Donor–acceptor treatment

DFT calculations were done on the SiR active site models following a previously established protocol.[2] Ground-state geometry optimizations[3] were performed with the resolution-of-identity approximation[4,5] using the TPSS[6] functional, the double-zeta level def2-SV(P) split-valence basis set[7] and Grimme's D3 correction for dispersion interactions[8]. Frequency calculations[9] were employed in order to assure that stationary points are true local minima. If significant imaginary frequencies were found, the molecular geometry was distorted along the coordinate involved the in imaginary vibration and the geometry optimization was redone. On each converged structure, single-point calculations were employed with the larger triple-zeta def2-TZVP basis set[10] using the B3LYP[11] functional. Solvation free energies were calculated with the COSMO[12] approach with optimized radii for all atoms[13] and 2.0 Å for Fe [14] (and a water solvent radius of 1.3 Å), setting the dielectric constant to $\varepsilon = 4$, mimicking a protein environment. The convergence criteria were set at 10^{-6} Hartree for the change in energy, 10^{-3} a.u. for the maximum displacement and maximum gradient element, while $5 \cdot 10^{-4}$ a.u. was set for their corresponding root-mean-square (RMS) change.

2. Non-equilibrium Green's function coupled with DFT (NEGF-DFT).

Based on the description of the electrode parts of the electron transport device, NEGF-DFT methods can be referred to as explicit, when the transport properties are computed by directly including the electrodes in the mathematical framework, and implicit when the electrode's presence is implied through a parameter (i.e. the Fermi energy of the electrode in eq. 5).

2.1 Molecular junction treatment (explicit NEGF-DFT)

Electron transmission was computed using the non-equilibrium Green's function method coupled with DFT (NEGF-DFT). The electronic structure of the island part together with the first layer of electrode atoms was treated with standard DFT, while semiperiodic DFT[15] was employed for the rest of the electrodes. This method is restricted to pure

functionals; consequently, the PBE functional was employed along with the DNP 3.5 basis set (with DFT semi-core pseudopotentials for Fe and Au).

The electron transmission from the source electrode (S) to the drain (D), $T_{SD,}$ is computed as the trace (Tr) of the matrix product of the right-hand side of equation 1:[16]

$$T_{SD}(E) = Tr[\Gamma_S(E)G^r(E)\Gamma_D(E)G^a(E)] \qquad (1)$$

where $\Gamma_{S/D}(E)$ represents the coupling matrix between the source (S) or drain (D) and the molecular junction and $G^{r/a}(E)$ the retarded (r) respectively advanced (a) Green's function of the molecular device. The results of this approach emphasize the difference in electron transmission capabilities between the two (siro)heme-cubane models. However, a more detailed view is obtained with the aid of the implicit approach, which allows the computation of the conductance between any two atoms comprising the molecular junction.

2.2 Electron route analysis (implicit NEGF-DFT)

The Green's function, as discussed in reference,[17] is defined as

$$[E - H(x)]G(x,x') = \delta(x,x') \qquad (2)$$

where E denotes the energy of the system, $G(x,x')$ is the Green's function and describes the electron's propagation from x to x', $\delta(x,x')$ is Dirac's delta function**,** and $\boldsymbol{H}(x)$ is the Hamiltonian operator with its dependence on the mass of electron, m, the position x and the potential in that point, $V(x)$, is given by:

$$H(x) = -\frac{1}{2m}\frac{\partial^2}{\partial x^2} + V(x)$$

.

This equation has two general solutions. The first one is called the retarded Green's function and has the form

$$G(x - x',E) = -\frac{i}{\vartheta}e^{ik|x - x'|} \qquad (3)$$

while the second, referred to as the advanced Green's function, is given by

$$G(x - x', E) = \frac{i}{\vartheta} e^{-ik|x - x'|} \qquad (4)$$

with $k = \sqrt{2m(E - V(x)}$

and $= \frac{k}{m}$.

In order to select one of the two solutions one can introduce an infinitesimal quantity, η, multiplied by the imaginary unit, *i*, and make the substitution, $E \rightarrow E \pm i\eta$, in order to obtain the retarded solution for the plus sign and the advanced solution for the negative sign.

Further developments of these equations for applications in the field of single-molecule electronics has led Yoshizawa[18] to use the following form proposed by Beratan[19]:

$$G_{rs}^{(0)R,A}(E_F) = \sum_k \frac{C_{rk} C_{sk}^*}{E_F - \varepsilon_k \pm i\eta} \qquad (5)$$

The left-hand side of this equation is a notation that describes the value of Green's function at the electrode's Fermi energy level (E_F) between an atom located on site *r* and another located on site *s*. The superscript notes that this is the zeroth order Green function, the order that describes the tunneling transmission, while *R* and *A* stands for the retarded and advanced forms. The right-hand side is a sum over all molecular orbitals (MO) spread over atoms *r* and *s*. *C* is the coefficient corresponding to the k^{th} MO, with *C** being its complex conjugate and ε_k the energy of the k^{th} MO.

The conductance expressed in eq. (5) can be further connected to the rate constant of the electron transfer reaction (k_{et}) by the expression developed by Nitzan:[20]

$$G = \frac{8e^2}{\pi^2 \Gamma_D \Gamma_A F} k_{et} \qquad (6)$$

where *G* is the conductance, *e* the charge of the electron, Γ_D the coupling between the electrode and the donor part of the junction, Γ_A the coupling between the electrode and the acceptor part of the junction, and *F* the thermally-averaged Franck–Condon-weighted density of states. By assuming typical experimental values for the couplings and the Franck–Condon factor it was further shown that the conductance and rate constant can be approximated as:

$$G \approx 10^{-17} k_{et} \qquad (7)$$

When implemented in the Multiwfn[21] quantum chemical software package, the $\pm i\eta$ term of equation (5) is neglected. For this reason, positive and negative values may both be computed. In this case, one sign corresponds to the direction from site *r* to *s* and the opposite sign corresponds to the opposite direction, from *s* to *r*. Thus, only the absolute value of the computed numbers is of importance. Furthermore, the current implementation in Multiwfn is limited to closed-shell systems. For this reason, the electron-route analysis was restricted to the ferrous (siro)heme–cubane systems and approximated as a closed-shell system. Nevertheless, the high-spin states were indirectly treated by taking extra MO in the summation part of eq. (5) up to LUMO+2. Although being approximative, the investigation does not focus on exact numerical values of the particular systems, but is rather concerned with the differences between the two variants of SiR active site, for which significant error cancelation can be expected.

For this treatment, the computations were performed at the B3LYP level of theory with the 6-311G(d,p) triple-zeta basis set for all atoms except Fe, for which the SDD basis set[22] was employed. This triple-zeta basis set was used due to technical limitations of the wave-function analysis program.

All calculations were performed with the use of Turbomole[23], Gaussian09[24] and DMol3[25] as implemented in Materials Studio[26], while wave-function analyses were done in Multiwfn[19] and Chemissian.[27] Protein visualizations were performed with the aid of Chimera.[28]

Explicit NEGF-DFT

Computed transmissions reveal crucial differences between the two (siro)heme–cubane models in terms electron transfer mechanism (Figure S3a). Thus, when computing the transmission probabilities for the clusterless models, it is observed that the broad peaks found in the –1.6 to 1 and 1–2 eV regions are higher in the siroheme case. This suggests a higher transmission between the island part (i.e. the molecular junction) and the electrode. At the Fermi energy, the opposite is valid, with heme possessing higher electron-transport capabilities. The sharp peaks present in the –2 eV region are much higher in the siroheme case, emphasizing a higher intra-molecular electron-transfer capability.

Proceeding to the (siro)heme-cubane systems (Figure S3b), it is observed that the peaks found in the –2 to –1.1 eV region are lowered when heme is replaced be siroheme,

while the peak associated with the state found in the –2.1 eV region becomes higher. The sharpness of these peaks suggests that these states are mostly localized on the island part of the device and, thus correspond to intramolecular charge transfer. Interestingly, these peaks reveal that some states involved in the intramolecular electron transfer process are inhibited while one of them is tuned such that the transmission of the electrons is increased. The broad peaks associated with the island–electrode charge transfer become lower in the –1.1 to –0.6 eV region and near the Fermi region when siroheme replaces the heme cofactor. The opposite effect is found in the –0.6 to –0.2 eV region and for all peaks situated above 0.1 eV. Again, siroheme increases the transmission of electrons in several states associated with the island–electrode charge transfer and decreases the transmission of other states. Overall, when siroheme instead of heme is connected to the cubane cofactor, some states involved in charge transfer process are inhibited while others become more favorable.

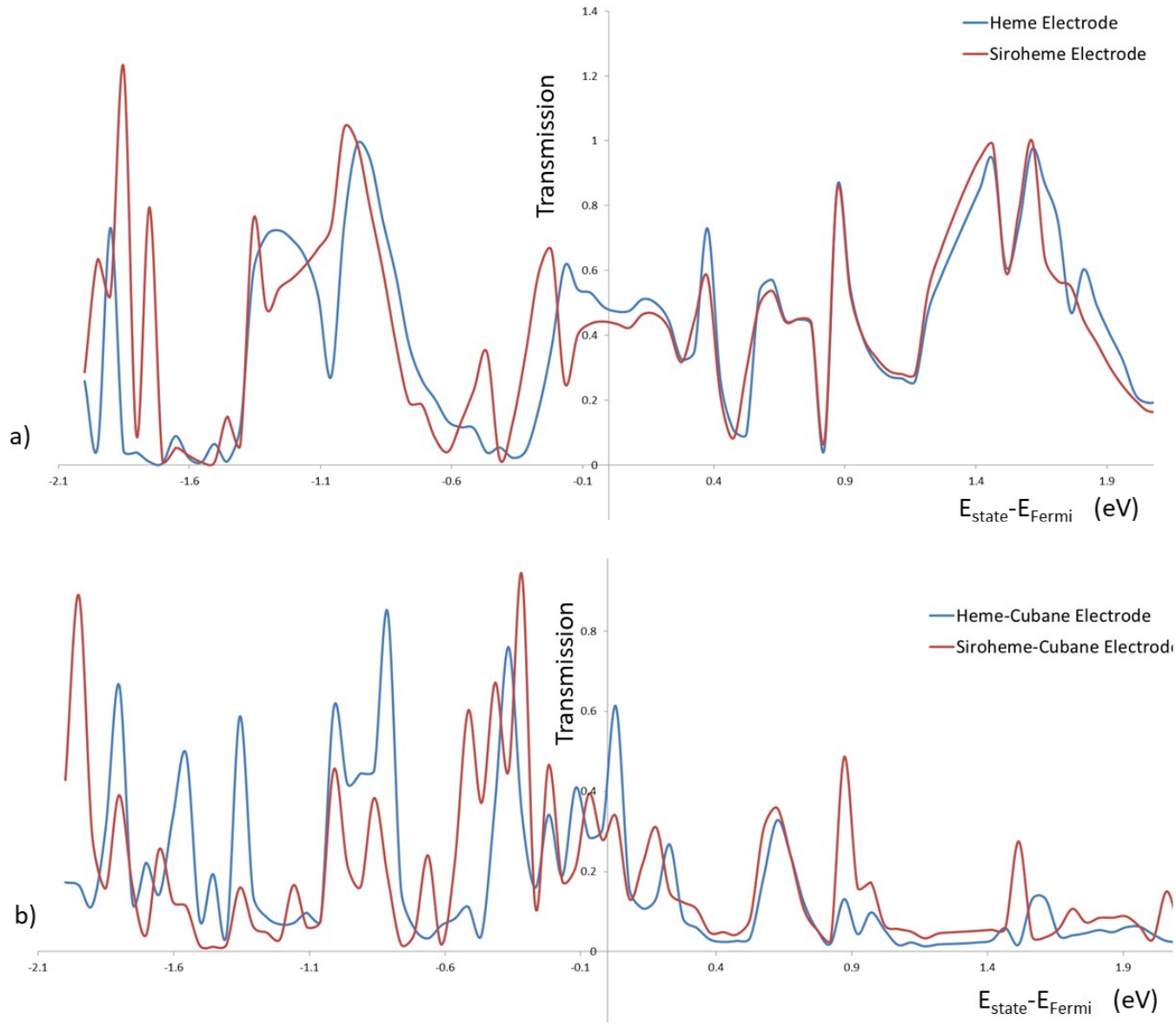

Figure S3. Electron transmission as a function of the energy associated with the electronic states involved in the charge transfer. The energy of the molecular state is expressed with reference to the electrode's Fermi energy. The blue line represents heme and the red line siroheme in a), and heme–cubane and siroheme–cubane in b). Transmissions are computed by the NEGF-DFT formalism at the PBE level with the DNP 3.5 basis set.

Intrinsic properties of the cubane cofactor

The Fe_4S_4 cubane behaves as an electron transmitter due to the high electron-transmission capabilities and to the non-bonding nature of its frontier orbitals with respect to the Fe–S bonds:[29] the HOMO orbitals (alpha and beta) are predominantly of metallic character (cf. Figure S4) while the LUMOs are of antibonding character with respect to the Fe–Fe interaction and possess high amplitudes also on the sulfur atoms (nonbonding character). Thus, by preserving its geometry upon the successive reduction and oxidation processes associated with the electron transfer, the cubane induces steric tension neither on its electron-providing residues nor on the siroheme system.

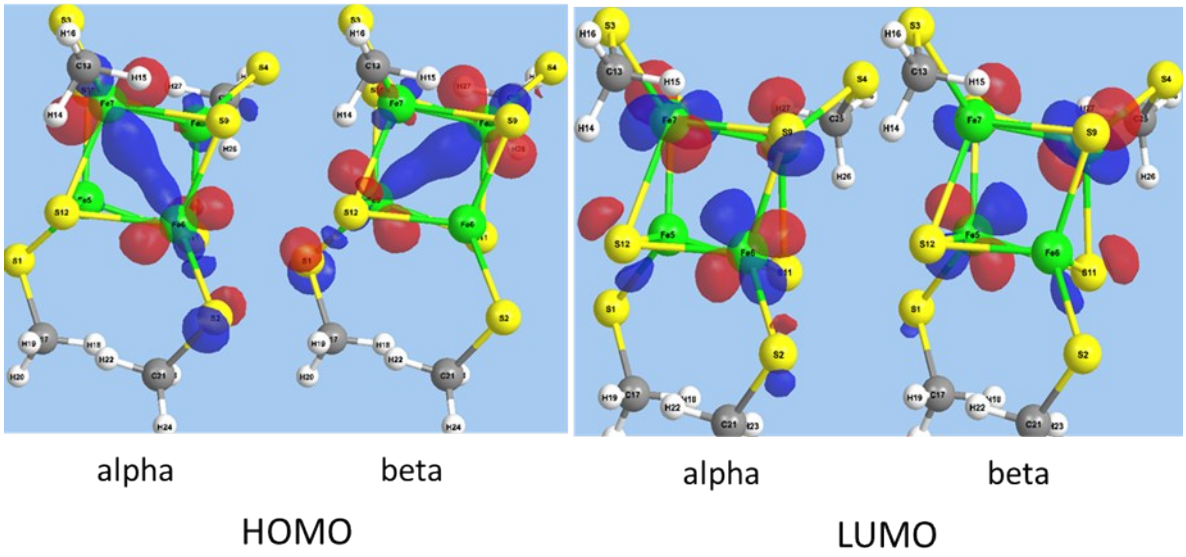

Figure S4. The HOMO (left) and LUMO (right) orbitals of the cubane cofactor computed at the B3LYP/def2-TZVP/COSMO(ε=4) level of theory.

Implicit NEGF-DFT

The conductance of the investigated routes was computed in several different orientations of the (siro)heme cofactor relative to the cubane (cf. Figure S5):

1) The geometry of active site as found in the crystal structure (pdb 1AOP) was used. This conformation is dubbed “Crystal, vertical geometry” in Figure S5. Models are depicted in Figure S6 and results are given in Table S1.
2) The geometry of the active was optimized. This conformation is dubbed “Crystal, relaxed geometry” in Figure S5. Models are depicted in Figure S7 while the results

are collected in Table S2. This geometry was further employed in the calculations reported in the main body of the article.

3) The geometry of the active site (as found in the crystal structure) was changed by orienting the two siroheme-specific saturated bonds towards the cubane cofactor. This conformation is dubbed "Facing, vertical geometry" in Figure S5. The distances between the two cofactors were kept as in the crystal structure. Models are depicted in Figure S8 and results are in Table S3.

4) The geometry of 3) was optimized. This conformation is dubbed "Facing, relaxed geometry" in Figure S5. Models are depicted in Figure S9 and results are collected in Table S4.

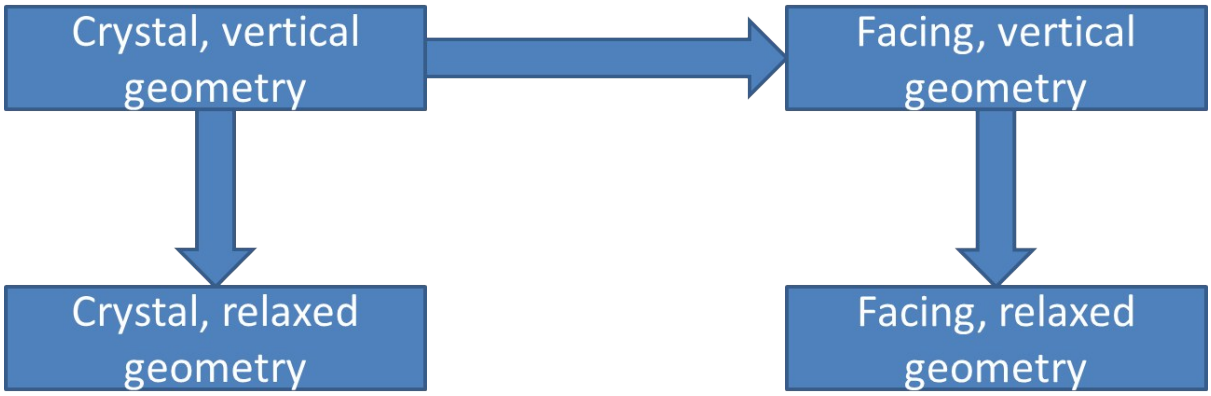

Figure S5. Scheme of the conformers used.

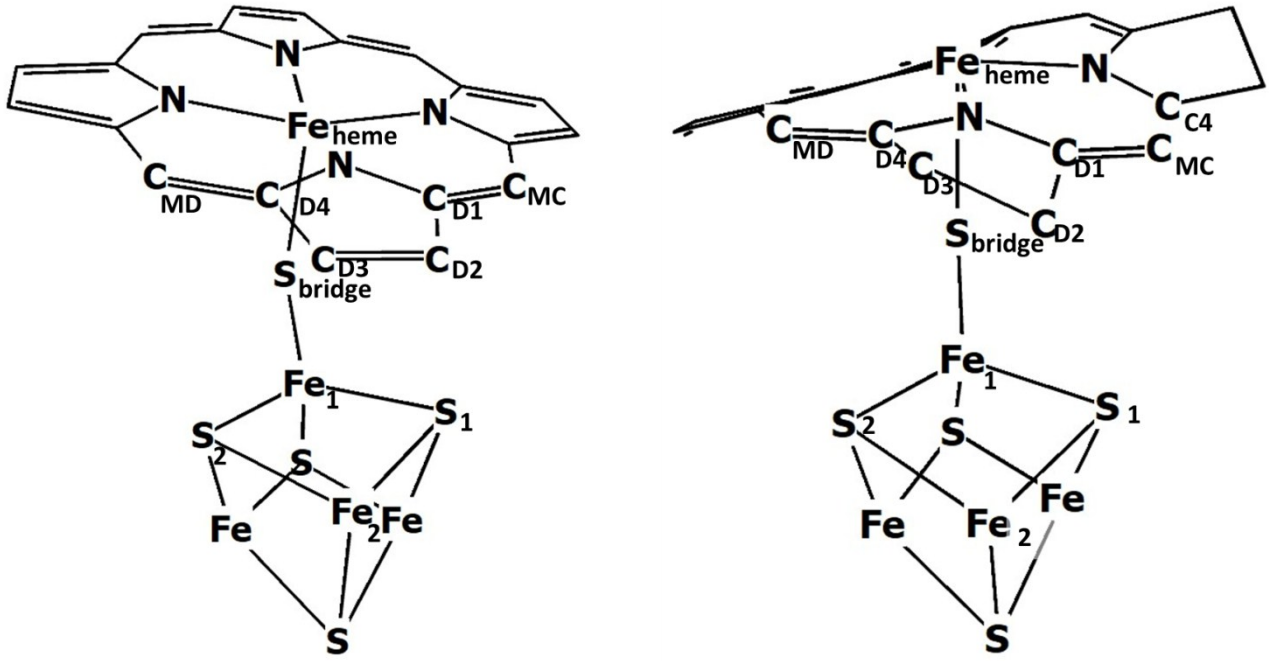

Figure S6. Heme–cubane (left) and siroheme–cubane (right) models in the "Crystal, vertical geometry" conformation.

Table S1. Computed conductance (*G*) for the investigated routes in the (siro)heme–cubane systems in the "Crystal, vertical geometry" conformation. Atom numbers are given in Figure S6, *d* represents the distance (in Å) between the two atoms.

Route	Heme-cubane				Siroheme-cubane			
	Atoms		*d*	*G*	Atoms		*d*	*G*
	#1	#2	(Å)		#1	#2	(Å)	
bridged	Fe_1	S_{bridge}	2.2	**2.2**	Fe_1	S_{bridge}	2.2	**2.3**
	S_{bridge}	Fe_{heme}	2.8	**1.6**	S_{bridge}	Fe_{heme}	2.8	**0.9**
direct	S_1	C_{MC}	3.6	0.3	S_1	C_{C4}	4.3	0.3
		C_{D1}	3.6	0.5		C_{MC}	3.6	0.3
		C_{D2}	3.8	0.5		C_{D1}	3.8	0.3
	Total			**1.3**	Total			**0.8**
direct	S_2	C_{D3}	3.8	0.2	S_2	C_{D3}	4.5	0.1
		C_{D4}	3.6	0.3		C_{D4}	4.1	0.2
		C_{MD}	3.7	0.4		C_{MD}	4.1	0.2
	Total			**0.8**	Total			**0.5**
direct	Fe_2	C_{D2}	3.8	0.1	Fe_2	C_{D2}	4.2	0.0
		C_{D3}	3.9	0.1		C_{D3}	5.0	0.1
	Total			**0.2**	Total			**0.1**
Total direct routes				**2.3**	Total direct routes			**1.4**

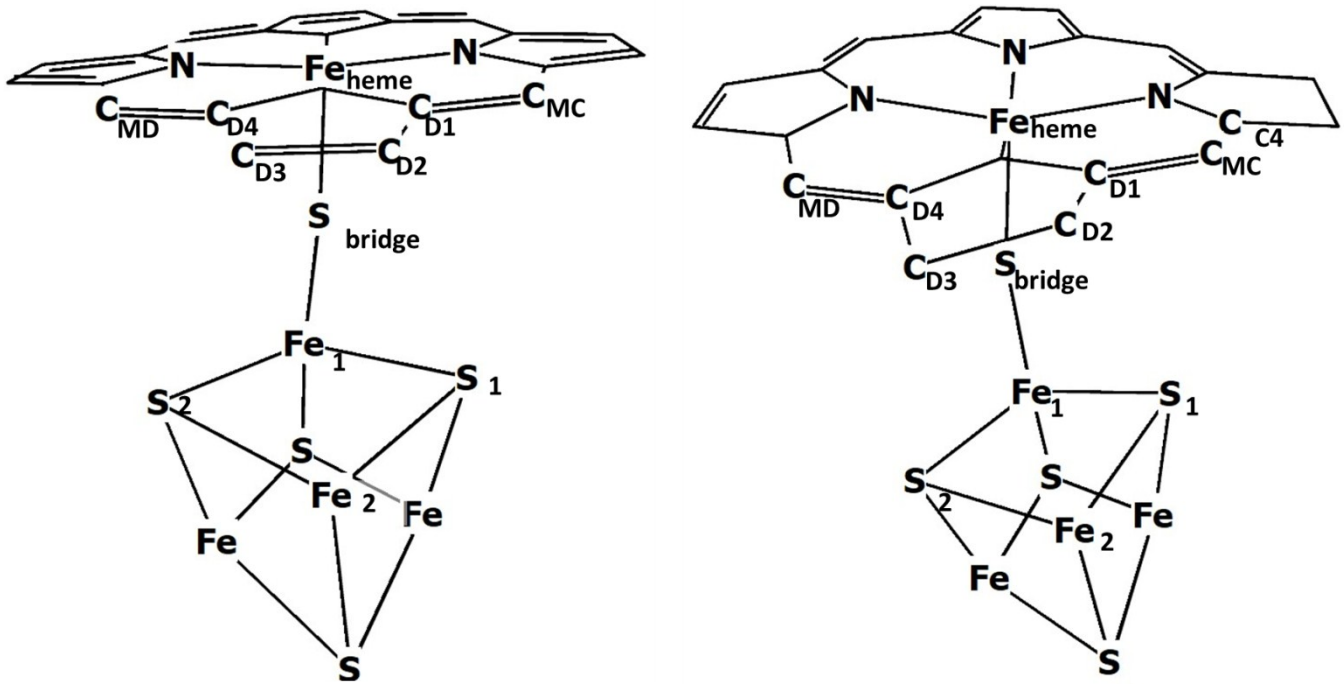

Figure S7. Heme–cubane (left) and siroheme–cubane (right) models in the "Crystal, relaxed geometry" conformation.

Table S2. Computed conductance (*G*) for the investigated routes in the (siro)heme–cubane systems in the "Crystal, relaxed geometry" conformation. Atom numbers are given in Figure S7 and *d* represents the distance (in Å) between the two atoms.

Route	Heme-cubane				Siroheme-cubane			
	Atoms		*d*	*G*	Atoms		*d*	*G*
	#1	#2	(Å)		#1	#2	(Å)	
bridged	Fe_1	S_{bridge}	2.4	**2.0**	Fe_1	S_{bridge}	2.3	1.9
	S_{bridge}	Fe_{heme}	2.2	**0.7**	S_{bridge}	Fe_{heme}	2.4	1.0
direct	S_1	C_{MC}	3.4	0.9	S_2	C_{C4}	3.6	0.2
		C_{D1}	3.3	1.3		C_{MC}	3.2	0.1
		C_{D2}	3.4	1.5		C_{D1}	3.4	0.1
	Total			**3.6**	Total			**0.4**
direct	S_2	C_{D3}	3.4	0.9	S_1	C_{D3}	3.7	0.3
		C_{D4}	3.4	0.9		C_{D4}	3.7	0.1
		C_{MD}	3.4	0.3		C_{MC}	4.0	0.2
	Total			**2.2**	Total			**0.6**
direct	Fe_2	C_{D3}	3.7	0.2	Fe_2	C_{D2}	4.0	0.2
		C_{D2}	3.7	0.1		C_{D3}	3.9	**0.1**
	Total			**0.3**	Total			**0.3**
Total direct routes				**6.1**	Total direct routes			**1.4**

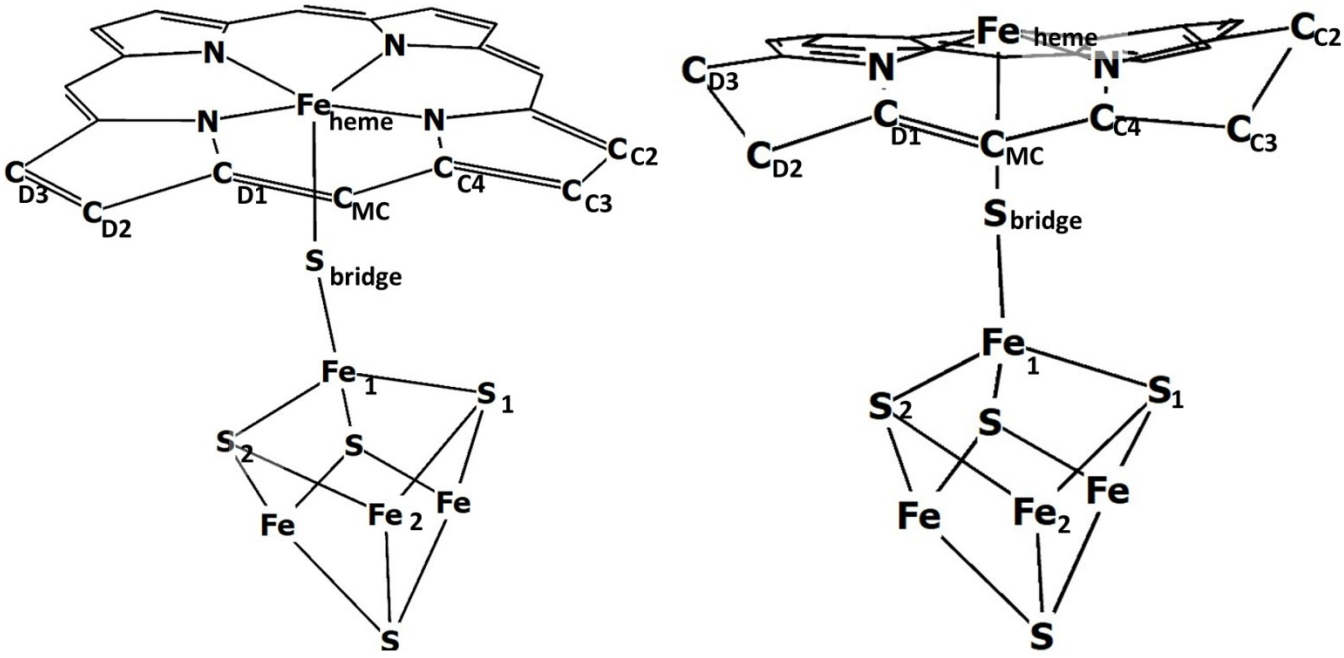

Figure S8. Heme–cubane (left) and siroheme–cubane (right) models in the "Facing, vertical geometry" conformation.

Table S3. Computed conductance (*G*) for the investigated routes in the (siro)heme–cubane systems in the "Facing,vertical geometry" conformation. Atom numbers are given in Figure S8 and *d* represents the distance (in Å) between the two atoms.

Route	Heme-cubane				Siroheme-cubane			
	Atoms		*d*	*G*	Atoms		*d*	*G*
	#1	#2	(Å)		#1	#2	(Å)	
bridged	Fe_1	S_{bridge}	2.2	**2.2**	Fe_1	S_{bridge}	2.2	**2.4**
	S_{bridge}	Fe_{heme}	2.8	**1.5**	S_{bridge}	Fe_{heme}	2.8	**0.6**
direct	S_1	C_{C2}	3.8	0.2	S_1	C_{C2}	4.8	0.1
		C_{C3}	3.5	0.6		C_{C3}	3.9	0.1
		C_{C4}	3.6	0.6		C_{C4}	3.8	0.6
	Total			**1.4**	Total			**0.8**
direct	S_2	C_{D1}	3.7	0.5	S_2	C_{D1}	3.8	0.4
		C_{D2}	3.7	0.3		C_{D2}	3.7	0.4
		C_{D3}	4.2	0.2		C_{D3}	4.8	0.1
	Total			**1.0**	Total			**0.9**
direct	Fe_2	C_{MC}	4.0	0.2	Fe_2	C_{MC}	4.4	0.1
Total direct routes				**2.6**	Total direct routes			**1.8**

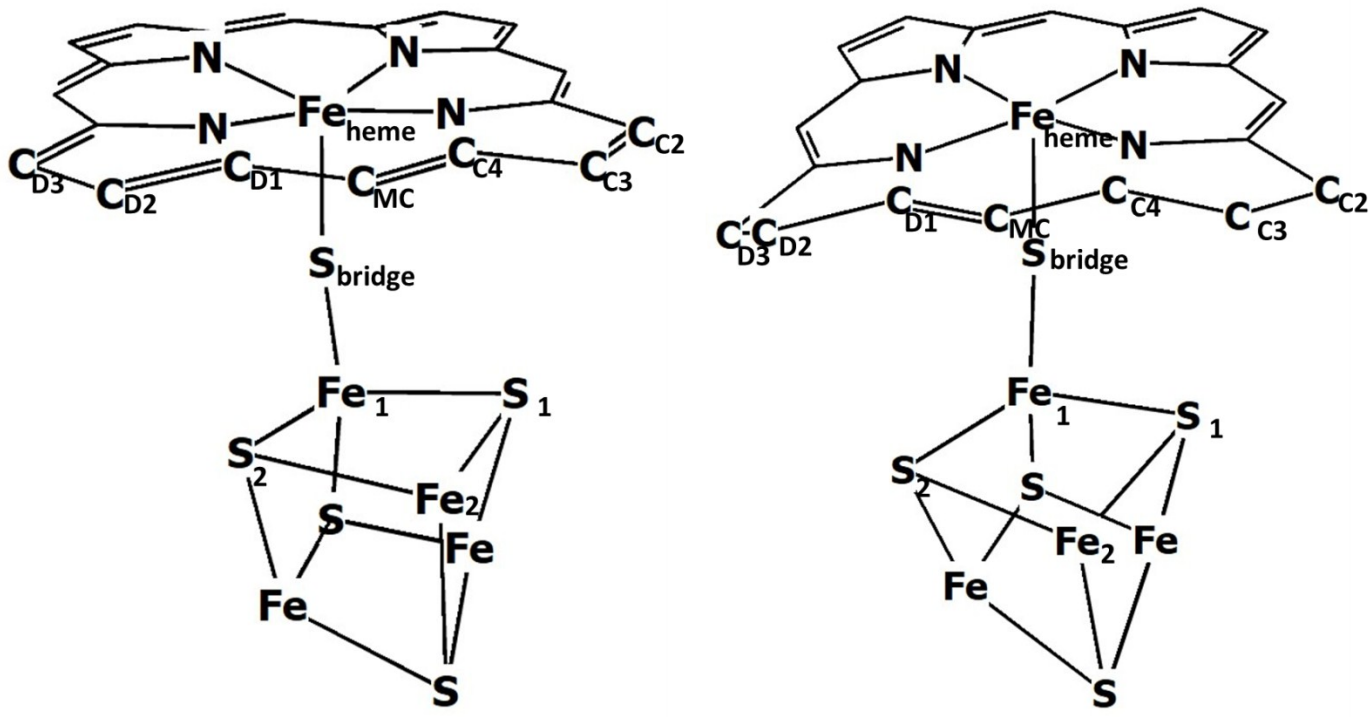

Figure S9. Heme–cubane (left) and siroheme–cubane (right) models in the "Facing, relaxed geometry" conformation.

Table S4. Computed conductance (*G*) for the investigated routes in the (siro)heme–cubane systems in the "Facing, relaxed geometry" conformation. Atom numbers are given in Figure S9 and *d* represents the distance (in Å) between the two atoms.

Route	Heme-cubane				Siroheme-cubane			
	Atoms		*d*	*G*	Atoms		*d*	*G*
	#1	#2	(Å)		#1	#2	(Å)	
bridged	Fe_1	S_{bridge}	2.3	**1.9**	Fe_1	S_{bridge}	2.3	**2.2**
	S_{bridge}	Fe_{heme}	2.4	**0.9**	S_{bridge}	Fe_{heme}	2.3	**0.8**
direct	S_1	C_{C2}	3.6	0.2	S_1	C_{C2}	3.4	0.2
		C_{C3}	3.4	0.4		C_{C3}	3.4	0.3
		C_{C4}	3.4	0.3		C_{C4}	3.3	0.6
	Total			**0.9**	Total			**1.1**
direct	S_2	C_{D1}	3.3	0.5	S_2	C_{D1}	3.3	0.6
		C_{D2}	3.4	0.4		C_{D2}	3.4	0.1
		C_{D3}	4.0	0.5		C_{D3}	3.6	0.1
	Total			**1.3**	Total			**0.8**
direct	Fe_2	C_{MC}	3.6	0.4	Fe_2	C_{MC}	3.8	0.1

Total direct routes	**2.6**	Total direct routes	**2.0**

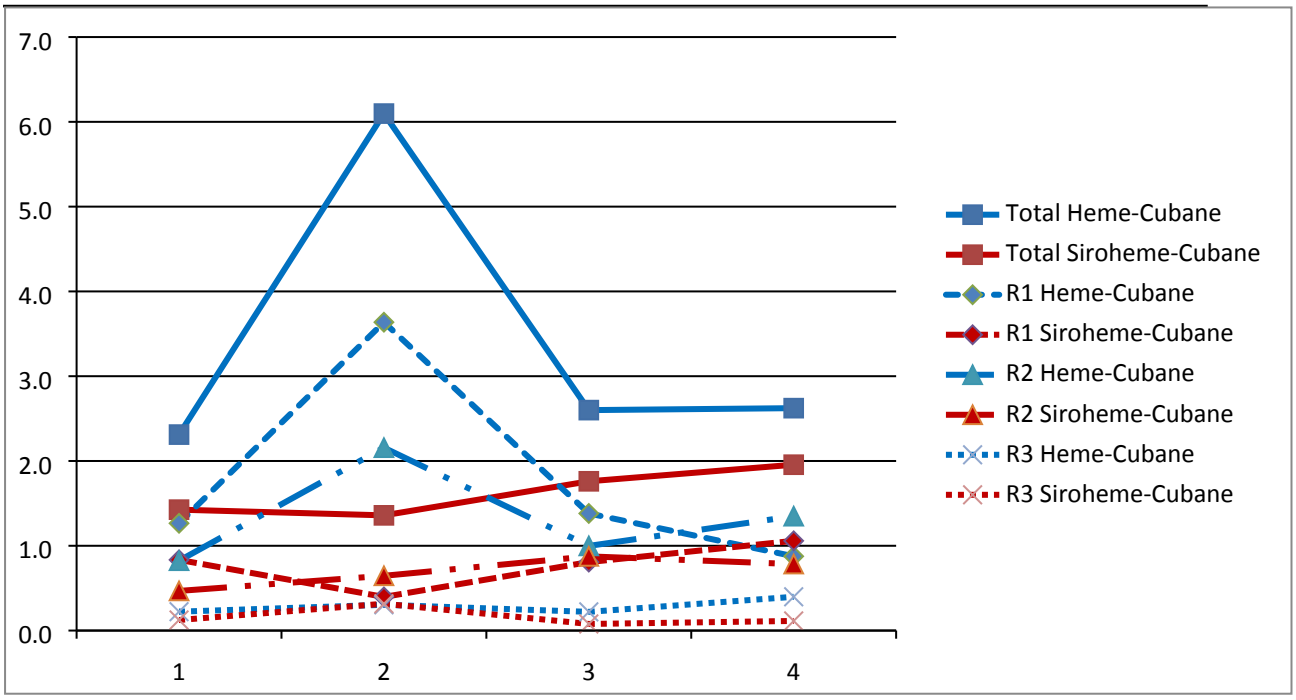

Figure S 10. Conductance in direct routes: 1= crystal, vertical geometry, 2= crystal, relaxed geometry, 3=facing, vertical geometry, 4= facing relaxed geometry

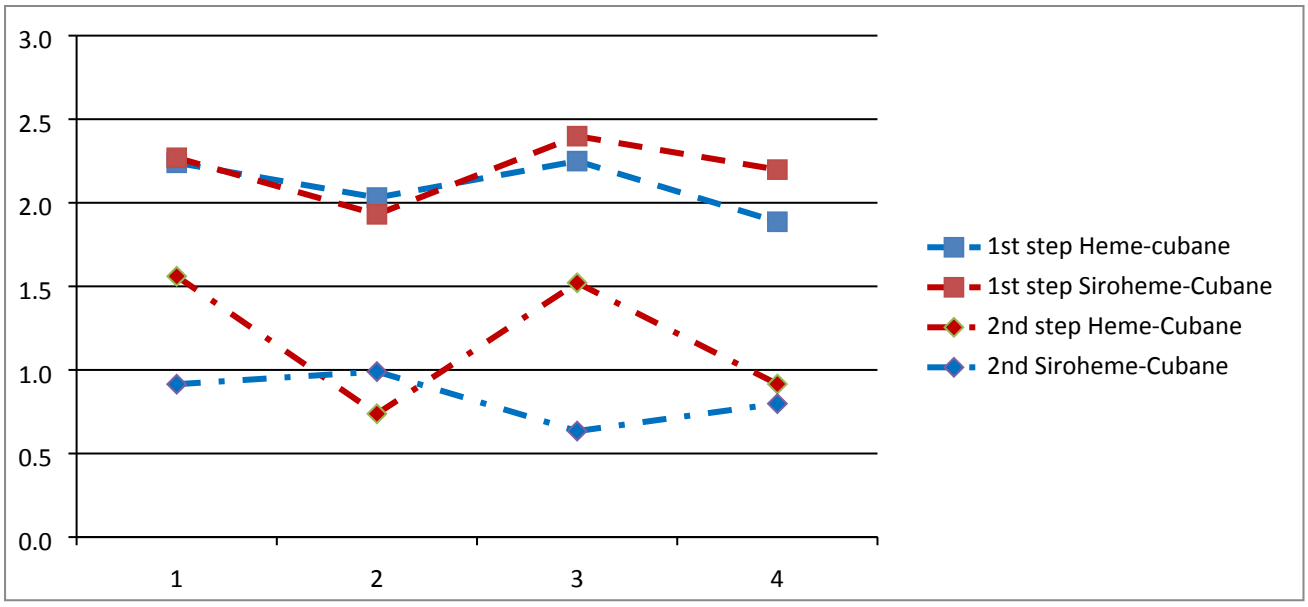

Figure S 11. Conductance in bridged route: 1= crystal, vertical geometry, 2= crystal, relaxed geometry, 3=facing, vertical geometry, 4= facing relaxed geometry.

Table 5. Energies of SiR active site different possible adopted geometries.

System	Geometry	Energy
		kcal/mol
Siroheme–Cubane	crystal vertical	0.0
	crystal relaxed	-74.0
	facing vertical	-78.1
	facing relaxed	-80.2

SiR active site as a donor–acceptor molecule

The two cofactors present in the SiR active site can be regarded as a donor–acceptor system that transfers electrons from the cubane moiety (the donor) to the siroheme moiety (the acceptor). In the resting state of SiR, both cofactors are in their oxidized state, i.e. with siroheme in the ferric state and the cubane cluster in the oxidised $[Fe_4S_4]^{2+}$ state. Before electron transfer, the cubane cluster needs to be reduced to the $[Fe_4S_4]^{+1}$ state. In the (siro)heme(ox)–cubane(red) state, the HOMO is located on the cubane cofactor and the LUMO on the (siro)heme cofactor (cf. Figure S13). However, the HOMO–LUMO gap (cf. Table 6) is increased when siroheme is used – apparently detrimental to internal electron transfer.

Treated separately, the LUMO of the donor fragment has to be located at a higher energy than the LUMO of the acceptor fragment such that, when a HOMO–LUMO excitation occurs, the transferred electron will end up on the acceptor fragment. According to the molecular orbitals in Figure S12, the LUMO of the isolated cubane is 2.64 eV above its HOMO, while the heme and siroheme LUMOs are at 0.30 and 0.41 eV above it, respectively. Upon changing from heme to siroheme, the LUMO is only slightly destabilized, whereas the HOMO is strongly destabilized, leading to a decrease of the HOMO–LUMO gap from 2.41 eV in heme to 1.95 eV in siroheme. However, the smaller difference between the heme HOMO and the cubane LUMO suggests that charge transfer associated with a HOMO–LUMO transition would be diminished in the siroheme–cubane variant.

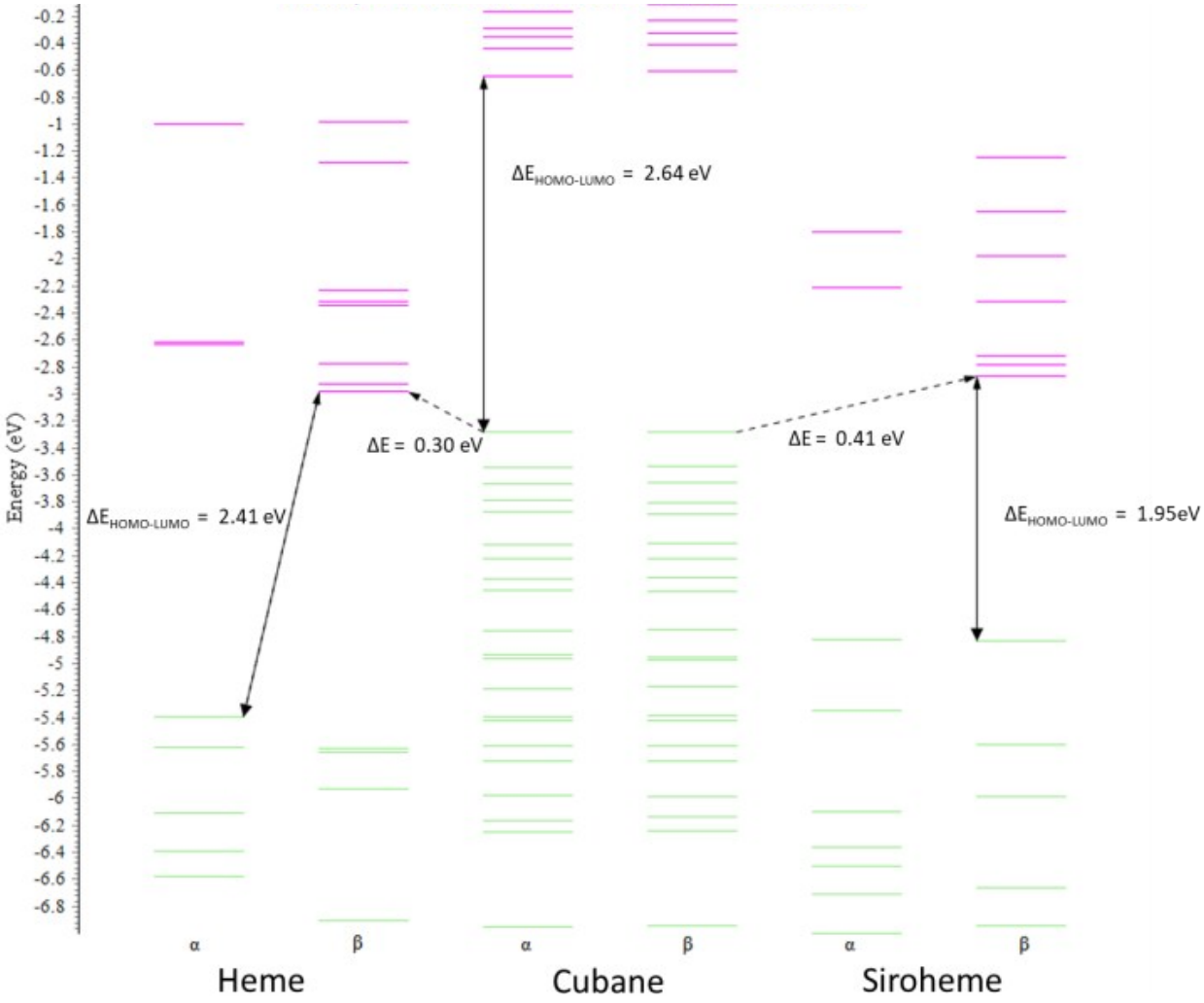

Figure S12. MO diagram of the isolated heme, cubane and siroheme fragments, computed at the B3LYP-D3/def2-TZVP level of theory for the ferric high-spin (siro)heme species and the dicationic form of the cubane cluster (reduced state). Occupied MOs are indicated in green lines while the virtual MOs in magenta.

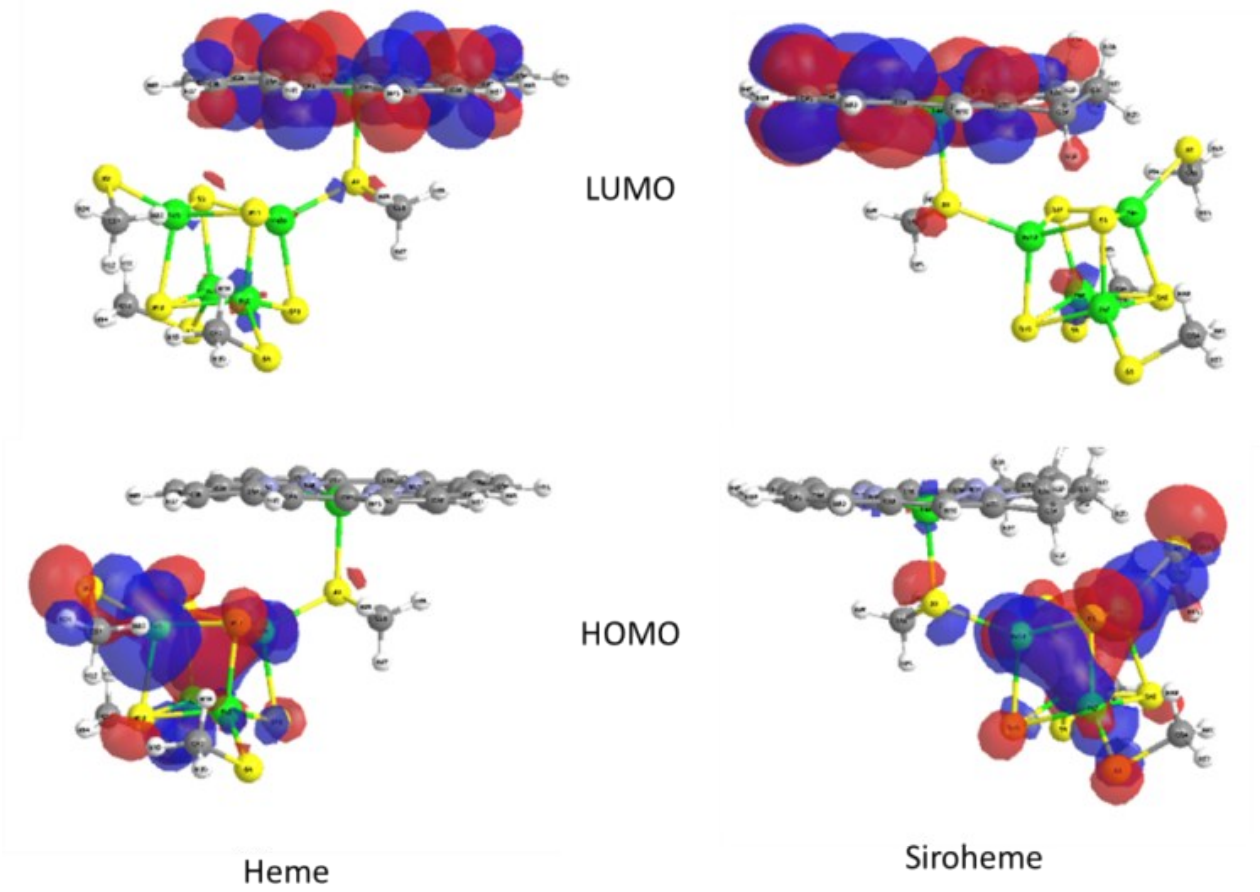

Figure S13. Frontier orbitals of the high-spin antiferromagnetically aligned heme–cubane and siroheme–cubane systems in the (siro)heme(ox)–cubane(red) state. Orbitals are computed at the B3LYP-D3/def2-TZVP/COSMO ε=4 level of theory.

Table 6. HOMO and LUMO levels and gaps. Values are computed at the B3LYP-D3/def2-TZVP/COSMO ε=4 level of theory.

System		HOMO (eV)	LUMO (eV)	Gap (eV)
Cubane		-3.28	-0.64	**2.64**
Heme		-5.39	-2.98	**2.41**
Siroheme		-4.82	-2.87	**1.95**
Heme(ox)-Fe_4S_4(red)	ferromagnetic	-2.93	-0.94	**1.99**
	antiferromagnetic	-2.93	-0.92	**2.01**
Siroheme(ox)-Fe_4S_4(red)	ferromagnetic	-2.95	-0.70	**2.25**
	antiferromagnetic	-2.91	-0.88	**2.03**

References

[1] A. Pecchia et al., "Non-Equilibrium Green's Functions in Density Functional Tight Binding: Method and Applications," *New Journal of Physics* 10, no. June (2008), https://doi.org/10.1088/1367-2630/10/6/065022.

[2] Adrian M.V. Brânzanic, Ulf Ryde, Radu Silaghi-Dumitrescu, "*Importance of the iron–sulfur component and of the siroheme modification in the resting state of sulfite reductase*", submitted.

[3] Oliver Treutler and Reinhart Ahlrichs, "Efficient Molecular Numerical Integration Schemes," *The Journal of Chemical Physics* 102, no. 1 (1995): 346–54, https://doi.org/10.1063/1.469408.

[4] K Eichkorn et al., "Auxiliary Basis Sets to Approximate Coulomb Potentials," *Chemical Physics Letters* 240, no. September (1995): 283–90, https://doi.org/http://dx.doi.org/10.1016/0009-2614(95)00838-U.

[5] Karin Eichkorn et al., "Auxiliary Basis Sets for Main Row Atoms and Transition Metals and Their Use to Approximate Coulomb Potentials," *Theoretical Chemistry Accounts: Theory, Computation, and Modeling (Theoretica Chimica Acta)* 97, no. 1–4 (1997): 119–24,

https://doi.org/10.1007/s002140050244.
[6] Jianmin Tao et al., "Climbing the Density Functional Ladder: Nonempirical Meta–Generalized Gradient Approximation Designed for Molecules and Solids," *Physical Review Letters* 91, no. 14 (2003): 146401–4, https://doi.org/10.1103/PhysRevLett.91.146401.
[7] Ansgar Schäfer, Hans Horn, and Reinhart Ahlrichs, "Fully Optimized Contracted Gaussian Basis Sets for Atoms Li to Kr," *The Journal of Chemical Physics* 97, no. 4 (1992): 2571–77, https://doi.org/10.1063/1.463096.
[8] Stefan Grimme et al., "A Consistent and Accurate Ab Initio Parametrization of Density Functional Dispersion Correction (DFT-D) for the 94 Elements H-Pu," *Journal of Chemical Physics* 132, no. 15 (2010), https://doi.org/10.1063/1.3382344.
[9] Peter Deglmann et al., "Nuclear Second Analytical Derivative Calculations Using Auxiliary Basis Set Expansions," *Chemical Physics Letters* 384, no. 1–3 (2004): 103–7, https://doi.org/10.1016/j.cplett.2003.11.080.
[10] Ansgar Schäfer, Hans Horn, and Reinhart Ahlrichs, "Fully Optimized Contracted Gaussian Basis Sets of Triple Zeta Valence Quality for Atoms Li to Kr," *The Journal of Chemical Physics* 100, no. 4 (1994): 5821–35, https://doi.org/10.1063/1.463096.
[11] Axel D. Becke, "Density-Functional Thermochemistry. III. The Role of Exact Exchange," *The Journal of Chemical Physics* 98, no. 7 (1993): 5648–52, https://doi.org/10.1063/1.464913.
[12] A. Klamt and G. Schüürmann, "COSMO: A New Approach to Dielectric Screening in Solvents with Explicit Expressions for the Screening Energy and Its Gradient," *J. Chem. Soc., Perkin Trans. 2*, no. 5 (1993): 799–805, https://doi.org/10.1039/P29930000799.
[13] Andreas Klamt et al., "Refinement and Parametrization of COSMO-RS," *Journal of Physical Chemistry A* 102, no. 26 (1998): 5074–85, https://doi.org/10.1021/jp980017s.
[14] Emma Sigfridsson and Ulf Ryde, "Comparison of Methods for Deriving Atomic Charges from the Electrostatic Potential and Moments," *Journal of Computational Chemistry* 19, no. 4 (1998): 377–95, https://doi.org/10.1002/(SICI)1096-987X(199803)19:4<377::AID-JCC1>3.0.CO;2-P.
[15] Alessandro Pecchia and Aldo Di Carlo, "Atomistic Theory of Transport in Organic and Inorganic Nanostructures," *Reports on Progress in Physics* 67, no. 8 (2004): 1497–1561, https://doi.org/10.1088/0034-4885/67/8/R04.
[16] Pecchia et al., "Non-Equilibrium Green's Functions in Density Functional Tight Binding: Method and Applications."
[17] Cuevas J.C., Scheer E., Molecular Electronics. An Introduction to Theory and Experiment, World Scientific, Singapore, 2010.
[18] Kazunari Yoshizawa, "An Orbital Rule for Electron Transport in Molecules," *Accounts of Chemical Research* 45, no. 9 (2012): 1612–21, https://doi.org/10.1021/ar300075f.
[19] Priyadarshy, S.; Skourtis, S. S.; Risser, S. M.; Beratan, D. N. Bridge-mediated electronic interactions: Differences between Hamiltonian and Green function partitioning in a non-orthogonal basis. J. Chem. Phys. 1996, 104 , 9473–9481.
[20] Abraham Nitzan, "A Relationship between Electron-Transfer Rates and Molecular Conduction," *Journal of Physical Chemistry A* 105, no. 12 (2001): 2677–79, https://doi.org/10.1021/jp003884h.
[21] Tian Lu and Feiwu Chen, "Multiwfn: A Multifunctional Wavefunction Analyzer," *Journal of Computational Chemistry* 33, no. 5 (2012): 580–92, https://doi.org/10.1002/jcc.22885.
[22] D. Andrae, U. Haussermann, M. Dolg, H. Stoll and H. Preuss, Theor. Chim. Acta, 1990, 77, 123
[23] TURBOMOLE V7.1 2016, a development of University of Karlsruhe and Forschungszentrum Karlsruhe GmbH, 1989-2007, TURBOMOLE GmbH, since 2007;

available from http://www.turbomole.com
[24] Frisch, M. J. et al. Gaussian 09, Revision E.01, Gaussian, Inc., Wallingford CT, 2013
[25] B. Delley, "An All-Electron Numerical Method for Solving the Local Density Functional for Polyatomic Molecules," *The Journal of Chemical Physics* 92, no. 1 (1990): 508–17, https://doi.org/10.1063/1.458452.
B. Delley, "From Molecules to Solids with the DMol3 Approach," *Journal of Chemical Physics* 113, no. 18 (2000): 7756–64, https://doi.org/10.1063/1.1316015.
[26] Dassault Systèmes BIOVIA, Materials Studio, 2017, San Diego: Dassault Systèmes, 2017
[27] L.V. Skripnikov, Chemissian Version 4.53, Visualization Computer Program, www.chemissian.com, 2017.
[28] UCSF Chimera--a visualization system for exploratory research and analysis. Pettersen EF, Goddard TD, Huang CC, Couch GS, Greenblatt DM, Meng EC, Ferrin TE. J Comput Chem. 2004 Oct;25(13):1605-12. http://www.rbvi.ucsf.edu/chimera .
[29] Louis Noodleman and David A. Case, "Density-Functional Theory of Spin Polarization and Spin Coupling in Iron-Sulfur Clusters," *Advances in Inorganic Chemistry* 38, no. C (1992), https://doi.org/10.1016/S0898-8838(08)60070-7.